Magnetic structure and analysis of the exchange interactions in $BiMO(PO_4)$ (M = Co, Ni)

2008 J. Phys.: Condens. Matter 20 415211

(http://iopscience.iop.org/0953-8984/20/41/415211)

J. Phys.: Condens. Matter **20** (2008) 415211 (9pp) doi:10.1088/0953-8984/20/41/415211

Magnetic structure and analysis of the exchange interactions in $BiMO(PO_4)$ (M = Co, Ni)

O Mentre[1,7], F Bouree[2], J Rodriguez-Carvajal[3], A El Jazouli[4], N El Khayati[5] and El M Ketatni[6]

[1] UCCS, Equipe de Chimie du Solide, UMR CNRS 8181, ENSC Lille–UST Lille, BP 90108, F-59652 Villeneuve d'Ascq Cedex, France
[2] Laboratoire Léon Brillouin [CEA-CNRS], CEA/Saclay, F-91191 Gif sur Yvette Cedex, France
[3] Institut Laue-Langevin, 6 rue Jules Horowitz, BP 156, F-38042 Grenoble Cedex 9, France
[4] LCMS, UFR Sciences des Matériaux Solides, Faculté des Sciences Ben M'Sik, Casablanca, Morocco
[5] Département de Physique, Faculté des Sciences, Avenue Ibn Batouta, BP 1014, Rabat, Morocco
[6] Laboratoire de Spectrochimie Analytique et Environnement, Faculté des Sciences et Techniques, Université Cadi Ayyad, BP 523, Béni Mellal, Morocco

E-mail: olivier.mentre@ensc-lille.fr

Received 20 March 2008, in final form 22 July 2008
Published 16 September 2008
Online at stacks.iop.org/JPhysCM/20/415211

Abstract

The magnetic structures of the two bismuth oxy-phosphate compounds $BiMPO_5$ ($M^{2+} = Ni^{2+}$, Co^{2+}) have been determined by neutron powder diffraction using group theory analysis as a preliminary tool. Both compounds adopt a monoclinic crystal structure (S.G. $P2_1/n$, $a = 7.1642(2)$ Å, $b = 11.2038(3)$ Å, $c = 5.1740(2)$ Å and $\beta = 107.296(2)°$ for Ni^{2+} and $a = 7.2441(1)$ Å, $b = 11.2828(1)$ Å, $c = 5.2258(1)$ Å and $\beta = 107.841(1)°$ for Co^{2+}). The refinement of the magnetic structures below $T_N = 17.5$ and 15 K, respectively, for both compounds show that the magnetic structure is characterized by the propagation vector $\mathbf{k} = (-1/2, 0, 1/2)$, with components given with respect to the reciprocal lattice of the nuclear structure. This means a magnetic unit cell that is a multiple of the nuclear cell. The magnetic structure is constituted of ferromagnetic pairs of metal ions antiferromagnetically coupled within double chains. The relative strength of the intra and inter double chains exchange interactions has been examined by establishing a theoretical magnetic phase diagram. Most of the interactions come from M–O–O–M super–super-exchange paths. At its ground state, $BiNiPO_5$ shows a nearly collinear arrangement of magnetic moments with $m_{1.5\,K} = 2.13(3)\ \mu_B$/Ni. Due to the strong magnetic anisotropy of Co^{2+} ($m_{1.5\,K} = 3.52(3)\ \mu_B$/Co), the collinear character is largely lost while the magnetic structure remains analysable on the basis of the greatest isotropic component of the local moments.

(Some figures in this article are in colour only in the electronic version)

1. Introduction

Compounds with the general formula $BiMPO_5$ (M = Co^{2+}, Ni^{2+}, Mn^{2+}, ...) [1–3] are very important from the topological point of view since they display the thinnest polycationic chain/ribbon-like almost systematically observed in compounds of the Bi_2O_3–MO–X_2O_5 ternary diagrams (M = Ni, Co, Cd, Pb, Mg, Ca, ... X = P, V, As ...) [4–7]. Therefore, according to an *'anti-structure'* description (based on edge sharing of oxo-centred $O(Bi, M)_4$ polyhedra models:

[7] Author to whom any correspondence should be addressed.

see [8] for more details) the crystal structure of the titular compounds displays infinite $[BiMO]^{3+}$ surrounded by PO_4^{3-} isolated tetrahedra. The $[BiMO]^{3+}$ chains are formed of edge-sharing $O(Bi_2M_2)$ tetrahedra with an $n = 1$ tetrahedron along their widths. Up to now, the $n = 1, 2, 3, 4, 5, 6, 11$ and ∞ terms have been isolated and characterized leading to clear relationships between the several compounds [9, 11]. Furthermore, in these chemical systems, this description type has been selected because it has proved to be strongly efficient to describe strongly disordered compounds in which the standard linkage of MO_x polyhedra was not viewable [8, 12]. From the magnetic point of view, this description type is all the more interesting, for instance yielding an easy observation of Cu^{2+} ($S = 1/2$) two-leg ladders in $BiCuPO_6$ formed between two adjacent $[BiCu_2O_2]^{3+}$ polycations, $n = 2$ tetrahedra wide [13]. It is obvious that the presence of PO_4 groups is also strongly important in the characterization of exchange interactions between paramagnetic centres. Since their corners are generally shared by several metallic cations, they mediate a competition between M–O–M super-exchange (SE) and M–O–O–M super–super-exchange (SSE) interactions. The latter are often underestimated but are, in fact, potentially very strong as recently evidenced in the AF magnetic ordering of $Ba_2Co_9O_{14}$ as soon as $T_N = 49$ K [14] with participation of Co^{2+}–O–O–Co^{2+} SSE paths (Co–Co > 5 Å). In the field of transition metal phosphates, numerous studies have considered independent magnetic M–M interactions on the basis of geometrical features, but these analyses often remain purely descriptive as in the case of $Fe_4(P_2O_7)_3$ where 38 interacting Fe^{3+}–Fe^{3+} direct, SE or SSE paths have been listed [15]. A more quantitative method to establish the hierarchy between the involved exchanges is to use numerical calculations. It yields the magnetic phase diagram adapted to the crystal type with the aim to set up a series of relative J values that are responsible for a ground state corresponding to the observed magnetic structure. The ground state or the first ordered state can be obtained by calculating the energy as a function of the **k** vectors within the first Brillouin zone [16–19]. The aim of this work is not to evaluate the exchange integrals but only the relative strengths of possible exchange interactions and, as a consequence, constraints between the J values are established to match with the ground state. This kind of calculation has been successfully applied to $MFePO_5$ (M = Fe, Co, Ni, Cu) [20, 21] and $CuFe_2(P_2O_7)$ [22] but it is noteworthy that the available algorithm only considers isotropic exchange interactions because anisotropy is expected to be relatively weak and contributes merely to orient the whole spin configuration with respect to the crystal lattice. Finally several comparable studies have been performed on materials interesting as positive electrode materials in Li-rechargeable batteries Li_3Fe_2, $(PO_4)_3$ [23] and $LiFe(P_2O_7)$ [24], also bringing nice elements of discussion about the effect of delithiation by comparison between $LiFePO_4$ and $FePO_4$ results [25]. In $LiFePO_4$, it is noteworthy that further electronic structure calculations validate the relative J values at the ground state [26]. In fact, the geometrical parameters (distances, angles, torsion angles, etc) determine the J values to a great extent. However, only qualitative arguments can be given about the relative strengths of the interactions (Goodenough–Kanamori–Anderson rules, hereafter GKA rules) in the absence of *ab initio* electronic structure calculations. Here, we have used this method for studying $BiMPO_5$ compounds (M = Co, Ni) through the group theory analysis and refinement of the magnetic structures. Due to complex crystal structure, restrictions based on topological considerations have been applied on independent exchange paths in order to simplify the analysis. They are discussed as well as the results of our calculations.

2. Experimental details

Polycrystalline samples of $BiMPO_5$ (M = Ni, Co) have been prepared by a standard solid state reaction method. Stoichiometric amounts of the high purity reactants Bi_2O_3 (Aldrich), NiO (Johnson Mathey, 99%), CoO (Aldrich, specpur) and $(NH_4)_2HPO_4$ (Fluka, puriss) were mixed and sintered at temperatures up to 950 °C for Ni and 850 °C for Co with several intermediate regrindings. The purity was checked by x-ray diffraction.

The magnetic susceptibility measurement from 5 to 300 K for $BiNiPO_5$ was carried out using a superconducting quantum interference device (SQUID) magnetometer.

Neutron powder diffraction data were collected on the G4.1 ($\lambda = 2.4266$ Å) and 3T2 ($\lambda = 1.2251$ Å) diffractometers at the Laboratoire Léon Brillouin (LLB, CEA Saclay). The high-resolution neutron powder diffractometer 3T2 allowed a precise determination of the nuclear crystal structures at room temperature. G4.1 data were used for the resolution of the magnetic structures in the low temperature domain up to 1.5 K.

The diffraction data were refined by the Rietveld method, using the FullProf 2000 software [27], and internal scattering lengths. A pseudo-Voigt function was used for describing the diffraction peak shapes. In order to refine the crystal structure we used as starting parameters those obtained by single-crystal x-ray diffraction [1, 2]. Each structural model was refined to convergence, with the best result selected on the basis of agreement factors and stability of the refinement.

The relative impact of the different exchange interactions on the magnetic structure was closely examined using the computer programs, SIMBO and ENERMAG that are briefly described in [21]. This analysis uses the approximation that the main features of the magnetic structure are determined by the isotropic exchange interactions, neglecting the sources of anisotropy (anisotropic exchange interactions and single-ion anisotropy).

3. Susceptibility measurements

The magnetic susceptibility measurements show a paramagnetic to antiferromagnetic transition at $T_N = 17.5$ K and 15 K for $BiNiPO_5$ (figure 1) and $BiCoPO_5$ [28]. respectively. In the paramagnetic region, the susceptibility data is modelled using a Curie–Weiss law: $\chi = C/(T - \theta_{CW})$ leading to $\theta_{CW} = -11.5$ K/ $-$ 62 K and $\mu_{eff} = 3.22\ \mu_B/5.40\ \mu_B$ for Ni and Co, respectively. For both compounds the

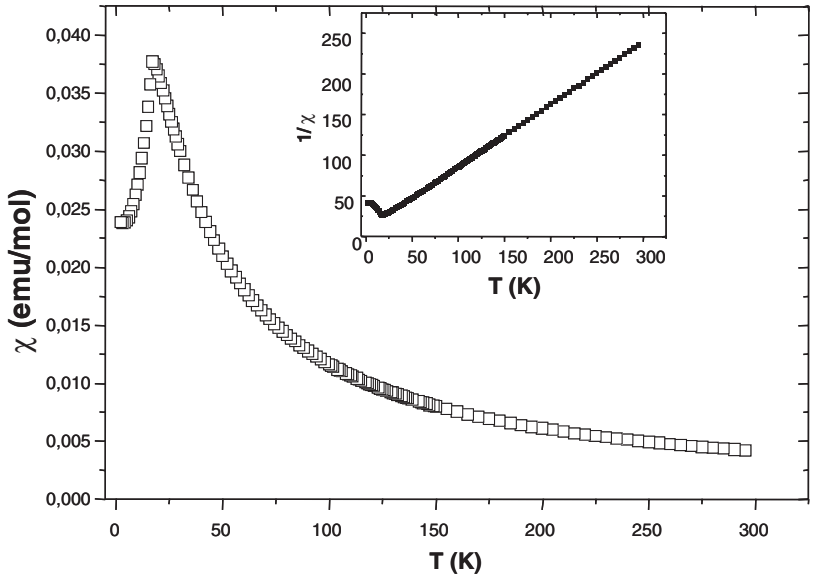

Figure 1. Plot of magnetic susceptibility versus T for $BiNiPO_5$. Inset: inverse susceptibility versus T.

effective moments are greater than expected in the spin-only consideration for Ni^{2+} ($S = 1$, $\mu_{eff} = 2.83\ \mu_B$) and Co^{2+} ($S = 3/2$, $\mu_{eff} = 3.87\ \mu_B$). These values indicate a certain degree of orbital contribution commonly observed, especially in the well-known case of cobalt cations. The spin–orbit coupling is responsible for the deviation from the collinear state of the ordered magnetic moments, to be discussed in the pertinent section. However, the θ_{CW} values are indicative of stronger AF exchange interactions in the Co^{2+} case, probably mediated by the greater magnetic moment for cobalt as compared to the nickel case. The deduction of the mean AF exchange interactions from the θ_{CW} values using the mean-field approximation is rather rash. Therefore, the magnetic structure and phase diagram analysis presented below will show the interplay of a number of distinct ferromagnetic (intra and inter M_2O_{10} dimers) and antiferromagnetic (inter dimers) exchange interactions that cannot be averaged.

4. Crystal structure

In a preliminary stage, the crystal structure of $BiMPO_5$ has been refined from neutron powder diffraction data (3T2 diffractometer, LLB, $\lambda = 1.2251$ Å) at room temperature. This refinement is efficient to check the purity of the powder and to validate the conservation of the atomic arrangement from the single crystal [1, 2] to the powder samples. The results of the refinement indicate a single-phase sample for M = Ni while in the M = Co case weak extra reflections indicate the presence of an unknown impurity phase. The corresponding regions have been excluded from the diffraction data. Both compounds are isomorphous and belong to the monoclinic crystal system with space group $P2_1/n$. The lattice and positional parameters and complementary data are listed in table 1. Table 2 reports the octahedral M–O distances as calculated from the 300 K and 1.5 K neutron data refinement. Only a slight contraction of the distances is observed. The structure is built up from a complex three-dimensional assembly of M_2O_{10} dimers linked by PO_4 groups, figure 2(a). As detailed in the introductory section, an alternative description displays infinite polycationic $[BiMO]^{3+}$ chains, formed of edge-sharing oxo-centred $O(Bi_2M_2)$ tetrahedra, one tetrahedron wide, running along c. They are surrounded by PO_4 groups, figure 2(b). The magnetic dimers are formed within one single chain. This viewing is practical to establish structural relationships between all compounds of the Bi_2O_3–MO–P_2O_5 phase diagram [8] and to highlight their magnetic specificities, e.g. BiM_2PO_6 compounds are formed of infinite $[BiM_2O_2]^{3+}$ ribbons, two tetrahedra wide, surrounded by PO_4 groups. In the $M = Cu^{2+}$ case, $S = 1/2$ two-leg ladders are formed between two ribbons [13].

5. Magnetic structure of $BiMPO_5$

In this section, the neutron data versus temperature collected on the G41 diffractometer ($\lambda = 2.4266$ Å) have been used. The lattice parameters have been refined while the structural parameters have been fixed to the room temperature values. Table 3 gathers the data collection and the refinement parameters. It is noteworthy that no structural modification is shown between room temperature and T_N. At this point, the magnetic satellites are observed in the neutron diffraction patterns. Their low angle parts measured on cooling are shown in figure 3. For both compounds, the growing reflections can be indexed according to a magnetic unit cell with lattice parameters $a_{magn} = 2a_{nucl}$, $b_{magn} = b_{nucl}$ and $c_{magn} = 2c_{nucl}$. Describing the magnetic structure with a propagation vector $\mathbf{k} = (-1/2, 0, 1/2)$ was selected with the aim that the first magnetic peak is indexed as $(0, 0, 0) \pm \mathbf{k}$. The propagation vector $\mathbf{k}' = (1/2, 0, 1/2)$ is also an equivalent alternative (i.e. $\mathbf{k}'$–$\mathbf{k}$ is a reciprocal lattice vector). The 4e Wyckoff site, occupied by M^{2+} cations, is constituted by four independent magnetic atoms within the unit cell

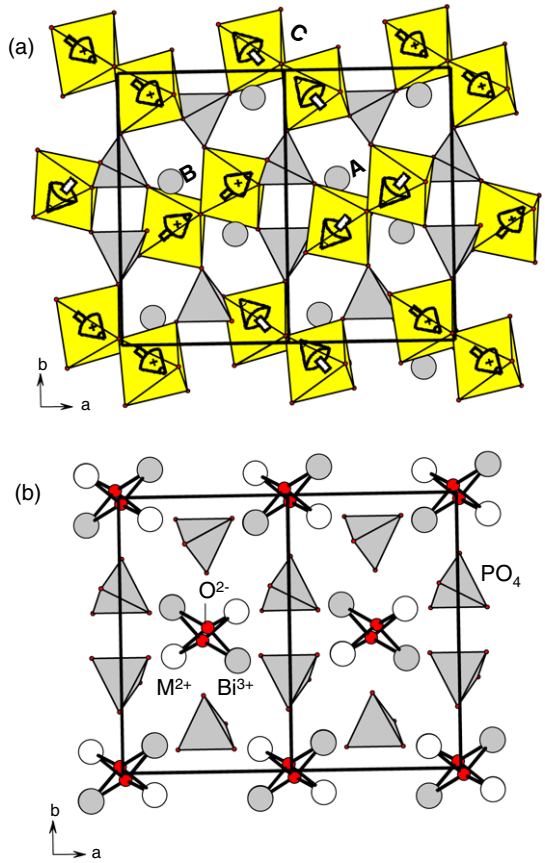

Figure 2. (a) Crystal and magnetic structures for $BiNiPO_5$ in terms of MO_6 and PO_4 polyhedra. (b) View of the $[BiMO]^{3+}$ chains surrounded by phosphates.

M_{1-4}. The magnetic structure was solved via Bertaut's symmetry analysis method [29] using BasIreps [30]. The 'global' magnetic representation Γ, associated with $P2_1/n$, (4e) and $\mathbf{k} = (-1/2, 0, 1/2)$ propagation vector, can be reduced upon four irreducible representations, each of them being one-dimensional, Γ_1 : (1 1 1 1), Γ_2 : $(11\bar{1}\bar{1})$, Γ_3 : $(1\bar{1}1\bar{1})$, Γ_4 : $(1\bar{1}\bar{1}1)$. The four 'numbers' (characters of the representations) in parentheses are associated respectively to the symmetry operators: 1, 2_1, −1 and n. As $\Gamma = 3\,(\Gamma_1 + \Gamma_2 + \Gamma_3 + \Gamma_4)$, three basis vectors are obtained for each Γ_i, leading to the four possible spin configurations below:

$$\Gamma_1:\ F^x = S_1^X + S_2^X + S_3^X + S_4^X;$$

$$G^Y = S_1^Y - S_2^Y + S_3^Y - S_4^Y;$$

$$F^Z = S_1^Z + S_2^Z + S_3^Z + S_4^Z$$

$$\Gamma_2:\ C^X = S_1^X + S_2^X - S_3^X - S_4^X;$$

$$A^Y = S_1^Y - S_2^Y - S_3^Y + S_4^Y;$$

$$C^Z = S_1^Z + S_2^Z - S_3^Z - S_4^Z$$

$$\Gamma_3:\ G^x = S_1^X - S_2^X + S_3^X - S_4^X;$$

Table 1. Atomic positions, unit cell parameters and $BiMPO_5$ (M = Ni, Co) determined from neutron diffraction at room temperature. A common B_{iso} value was refined for all atoms: M = Ni: 0.641(8) $Å^2$; M = Co: 0.65(2) $Å^2$.

S.G.		$P2_1/n$	
		$BiNiPO_5$	$BiCoPO_5$
a (Å)		7.1642(2)	7.2441(1)
b (Å)		11.2038(3)	11.2828(1)
c (Å)		5.1740(2)	5.2258(1)
β (deg)		107.296(2)	107.841(1)
Ang. range (deg)		$6 \leqslant 2\theta \leqslant 125$	(λ = 1.225 Å)
R_p (%)		6.15	6.04
R_{wp} (%)		6.91	6.20
R_{Bragg} (%)		3.39	2.87
R_F (%)		2.19	1.63
χ^2		3.13	1.95
Bi	x	0.1904(3)	0.1914(3)
	y	0.0991(2)	0.0978(2)
	z	0.1103(4)	0.1131(4)
M	x	0.8131(3)	0.8131(9)
	y	0.0803(2)	0.0864(6)
	z	0.3700(4)	0.371(1)
P	x	0.0212(4)	0.0207(4)
	y	0.3475(3)	0.3478(3)
	z	0.2184(7)	0.2170(6)
O1	x	0.3381(4)	0.3389(4)
	y	0.9180(3)	0.9186(2)
	z	0.0456(5)	0.0530(5)
O2	x	−0.0146(4)	−0.0126(4)
	y	0.2222(3)	0.2237(2)
	z	0.3139(6)	0.3137(5)
O3	x	0.8282(4)	0.8306(4)
	y	0.4182(3)	0.4179(2)
	z	0.1132(5)	0.1086(5)
O4	x	0.4836(5)	0.4840(4)
	y	0.4760(3)	0.4773(2)
	z	0.2458(7)	0.2472(6)
O5	x	0.6110(4)	0.6080(4)
	y	0.1719(3)	0.1719(2)
	z	0.4854(6)	0.4850(5)

$$F^Y = S_1^Y + S_2^Y + S_3^Y + S_4^Y;$$

$$G^Z = S_1^Z - S_2^Z + S_3^Z - S_4^Z$$

$$\Gamma_4:\ A^X = S_1^X - S_2^X - S_3^X + S_4^X;$$

$$C^Y = S_1^Y + S_2^Y - S_3^Y - S_4^Y;$$

$$A^Z = S_1^Z - S_2^Z - S_3^Z + S_4^Z$$

where $S_i^{X,Y,Z}$ are the components along **a**, **b** or **c** of the magnetic moment of atom i (cf table 4). The symbols $A(+--+)$, $C(++--)$, $F(++++)$ and $G(+-+-)$ correspond to Bertaut's notations [29] for sequences of four parallel magnetic moments. The magnetic models corresponding to the four representations have been tried by least-squares refinement. The best agreement was obtained for a magnetic structure corresponding to the irreducible

Table 2. Octahedral M–O bonds for $BiMPO_5$ (M = Ni, Co) from neutron powder diffraction data at 1.5 and 300 K.

		1.5 K	300 K
M–O(1)	Ni	2.102(17)	2.101(3)
	Co	2.136(13)	2.156(5)
M–O(2)	Ni	2.076(15)	2.085(4)
	Co	2.082(14)	2.086(6)
M–O(3)	Ni	2.085(16)	2.094(4)
	Co	2.186(12)	2.173(6)
M–O(4)	Ni	2.076(16)	2.064(4)
	Co	2.088(13)	2.094(6)
M–O(4)	Ni	2.086(14)	2.089(4)
	Co	2.110(16)	2.144(6)
M–O(5)	Ni	1.998(17)	2.005(4)
	Co	2.045(16)	2.009(6)

Table 3. Crystal and refinement data at 1.5 K for $BiMPO_5$. For M = Co the excluded regions contain unassigned impurity lines.

	$BiNiPO_5$	$BiCoPO_5$
a (Å)	7.1614(3)	7.2525(3)
b (Å)	11.1947(4)	11.2893(4)
c (Å)	5.1682(2)	5.2300(2)
α (deg)	90.0	90.0
β (deg)	107.308(2)	107.846(2)
γ (deg)	90.0	90.0
Ref. domain	10–90	$[12-15.7]\cup$ $[17.38-36.31]\cup$ $[36.9-90]$
2θ step (deg)	0.05	0.05
Profile parameters U	0.83(4)	0.92(4)
V	−0.33(4)	−0.42(4)
W	0.098(9)	0.135(7)
Temperature (K)	1.5	1.4
No. free parameters	38	38
R_p (%)	9.16	7.81
R_{wp} (%)	9.75	8.65
R_{Bragg} (%)	2.09	2.70
R_F (%)	2.06	1.89
Magn. R factors (%)	11.7	7.15

representation Γ_2. The magnetic structure was refined, using the space group $P\bar{1}$ for generating the magnetic satellites in half the reciprocal space, as an extra phase containing only the M^{2+} paramagnetic centres with constraints between magnetic components imposed by the tested representation. The free parameters of refinements at 1.5 K are listed in table 3. The refined magnetic components and the atomic coordinates that define M_{1-4} are listed in table 4. It is well known that transition metal oxides can exhibit local magnetic moments on oxygen atoms but their contribution to the magnetic powder diffraction pattern is negligible (low moment and magnetic form factor decreasing very fast with scattering angle) so, hereafter, no moments in oxygen atoms have been considered.

M = Ni: the final magnetic reliability is $R_{mag} = 11.7\%$ (or 5.17% in a working range limited to $2\theta = 40°$). It yields a total magnetic moment of 2.13(3) μ_B/Ni^{2+} which is slightly greater than its expected value of 2 μ_B in the spin-only approximation. Normally, covalence effects and/or zero-point spin reduction [31] should decrease the expected value. The spin–orbit coupling is probably responsible for this high value as well as the existence of anisotropic magnetic interactions.

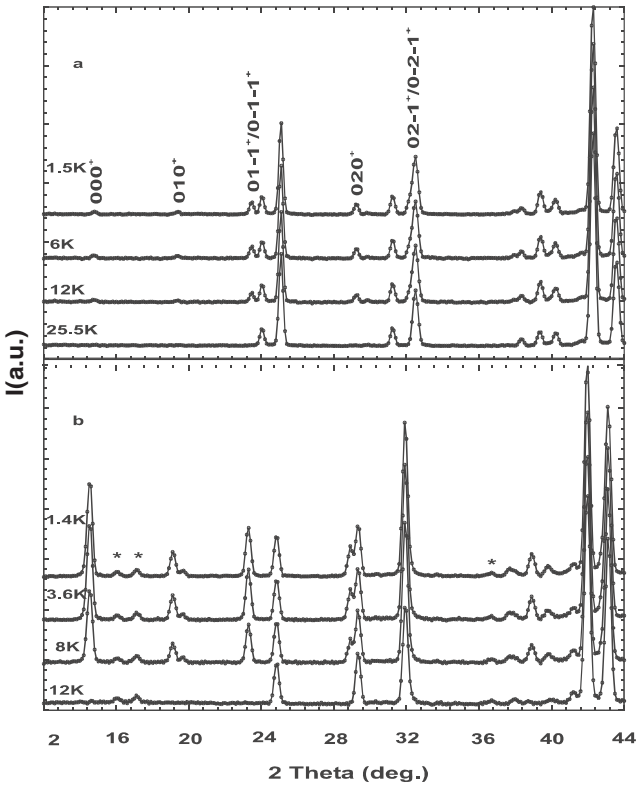

Figure 3. Thermal evolution of the low angle part of the neutron powder patterns (λ =2.427Å) of $BiMPO_5$ with indexing of the main magnetic satellites for $\mathbf{k} = (-1/2, 0, 1/2)$ and (a) M = Ni, (b) M = Co.

However, it is noteworthy that the structure is roughly collinear to the c axis since $\mathbf{M}_z \gg \mathrm{M}x$, $\mathbf{M}_y$. The projection of the magnetic structure along c is shown in figure 2(a) with moments mostly perpendicular to the plane of representation. This projection enables us to distinguish double chains (d.c.) made of M_2O_{10} dimers interconnected by PO_4 groups running along c. Here, the central d.c. called A is interacting with two d.c. of type B and four d.c. of type C. This scheme is helpful to distinguish the magnetic interactions in competition in the crystal. The thermal evolution of the refined moments for the two compounds is shown in figure 4. It shows that there is no change in the spin configuration in the magnetic ordered temperature domain.

M = Co: in this case the magnetic peaks, appearing below 12 K (figure 3(b)), consist of more intense lines that can be indexed using the propagation vector $\mathbf{k} = (-1/2, 0, 1/2)$. The data were treated in the same manner, also leading to the best agreement for representation Γ_3. At 1.5 K the final R_{magn} is 7.15% while $\mu Co^{2+} = 3.52(3)\ \mu_B$ that suggests an orbital contribution of ∼0.5 μ_B, in good agreement with the μ_{eff} value. In this case the structure is clearly non-collinear anymore according to the three components $\mathbf{M}_x > \mathbf{M}_y > \mathbf{M}_z$. However, one should remark from the values of table 4 that the largest components, $\mathbf{M}_z$ (Ni case) and $\mathbf{M}_x$ (Co case), both adopt the $C(++--)$ configuration. This will be particularity helpful for the determination of a unique approximate phase diagram common to both compounds.

Table 4. Coordinates of the magnetic atoms M_{1-4} in the crystal cell and refined magnetic components (μ_B) for $BiMPO_5$ at 1.5 K, $\mathbf{k} = (-1/2, 0, 1/2)$.

	Atomic positions			Magnetic components (μ_B)		
Atom	**x**	**y**	**z**	$\mathbf{M}_x$	$\mathbf{M}_y$	$\mathbf{M}_z$
M(1) Ni	x	y	z	−0.54(3)	0.33(4)	1.89(3)
Co				2.89(3)	1.32(4)	−0.78(4)
M(2) Ni	$-x+3/2$	$y+1/2$	$-z+1/2$	−0.54(3)	−0.33(4)	1.89(3)
Co				2.89(3)	−1.32(4)	−0.78(4)
M(3) Ni	$-x+1$	$-y+1$	$-z+1$	0.54(3)	−0.33(4)	−1.89(3)
Co				−2.89(3)	−1.32(4)	0.78(4)
M(4)Ni	$x-1/2$	$-y+1/2$	$z+1/2$	0.54(3)	0.33(4)	−1.89(3)
Co				−2.89(3)	1.32(4)	0.78(4)

Table 5. Geometrical parameters of the magnetic exchange interactions in $BiMPO_5$ (M = Ni, Co) ordered by analogy to figure 5.

	n. paths	Mult.		M–O	O–O′	O′–M	M–O–O′	O–O′–M	M–O–M	Torsion (deg)	M–M
J_1	(2×) M–O(4)–M	1	Ni	2.064	2.678	2.089			99.71		3.174
			Co	2.089	2.713	2.144			100.4		3.256
J_2	(1×) M–O(1)–O(5)–M	2	Ni	2.101	2.551	2.005	149.4	99.8		84.9	5.174
			Co	2.156	2.542	2.009	148.4	99.9		87.3	5.226
J_4	(2×) M–O(1)–O(3)–M	1	Ni	2.101	2.514	2.094	144.2	110.0		66.39	5.273
			Co	2.156	2.504	2.173	143.4	109.7		69.3	5.353
J_5	(2×) M–O(3)–O(5)–M	1	Ni	2.094	2.521	2.005	142.5	125.5		5.56	5.363
			Co	2.173	2.512	2.009	143.0	126.8		5.51	5.462
J_3	(1×) M–O(3)–O(2)–M	2	Ni	2.094	2.544	2.085	153.2	120.4		73.6	5.751
			Co	2.173	2.552	2.086	152.3	119.6		70.6	5.794
J_7	(1×) M–O(2)–O(1)–M	2	Ni	2.085	2.528	2.101	152.5	111.3		43.4	5.336
			Co	2.086	2.524	2.156	152.1	108.6		45.6	5.285
J_8	(1×) M–O(5)–O(2)–M	2	Ni	2.005	2.453	2.085	154.2	145.0		144.7	6.284
			Co	2.009	2.456	2.086	153.2	145.3		143.5	6.287

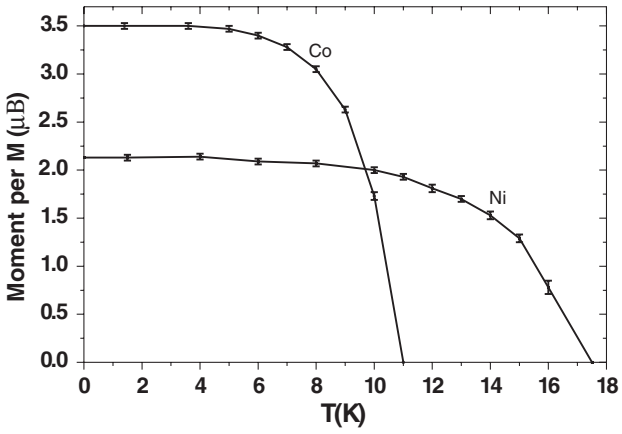

Figure 4. Thermal variation of the Ni^{2+} and Co^{2+} magnetic moments in $BiNiPO_5$.

6. Magnetic phase diagram

In this section, the selected propagation vector has been changed to $\mathbf{k} = (1/2, 0, 1/2)$ for convenience to use the different programs described below. Of course, this transformation does not affect the validity of the refined magnetic structure. As a first step to access the magnetic phase diagram, we need to identify the different M—M interactions existing in the particular topology corresponding to the crystal structure under study. This topological analysis can be performed with the help of the program SIMBO that needs the structural data as input. Calculations were performed neglecting the M–M separations greater than 6.3 Å since there is a gap in distances between 6.28 and 7.16 Å. Starting from a central M^{2+} cation, eight isotropic independent exchange interactions are found and listed in ascending order of distances in table 5 with their geometrical characteristics including the number of equivalent paths from a central M1 to the neighbouring M2, and the multiplicity defined by the number of equivalent M2 sites around the central M1. In fact, each M1 is magnetically interacting with 11 M2 neighbours via 14 paths. It highlights the complexity of the magnetic interplay. In this list, J_6 as been skipped since it does not involve any M–O–O–M orbital overlapping. The other can be gathered into three distinct groups, as evidenced in figure 5.

(i) J_1 and J_2 both involve intra double chain exchange paths, J_1 (moments connected by J_1 are parallel) being efficient through edge-sharing octahedra (double M–O–M SE path with possible participation of direct M–M exchange) and J_2 (moments connected by J_2 are antiparallel) corresponds to interactions through M–O–O–M super-exchange paths running along the chain axis, figure 5(a). Considering the distances, both exchange integrals are supposed to be strong. Furthermore, the M–O–M angle being close to 90°, the GKA rules predict for both $M = Ni^{2+}$ ($t_{2g}{}^6e_g{}^2$, $S = 1$) and Co^{2+} ($t_{2g}{}^5e_g{}^2$, $S = 3/2$) a positive J_1. This interaction appears to be satisfied in the magnetic

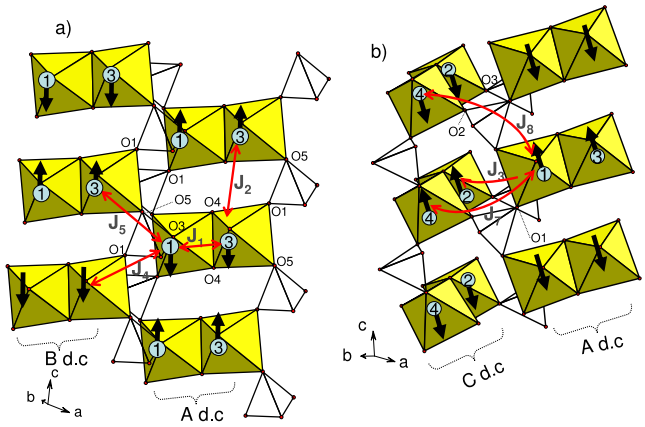

Figure 5. Representation of the exchange paths between the Ni^{2+} cations. (a) J_1, J_2 intra double chains (d.c.) and J_4, J_5 inter A–B d.c. exchange interactions. (b) J_3, J_7, J_8 inter A–C d.c. exchange interactions. A, B and C entities are defined in figure 2(a).

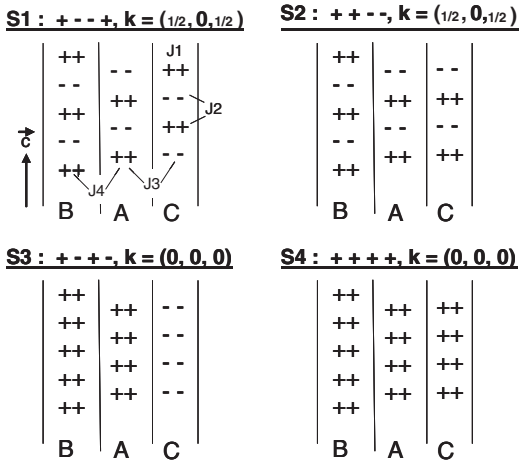

Figure 6. Scheme of the magnetic orderings between double chains A, B and C associated with the structures S1–S4. In this figure, A, B and C, are arranged by analogy to figures 5(a) and (b).

structure, where the M_1–M_3 ions have their moments parallel. Then J_1 will be set to unity and taken as a reference for the phase diagram calculation.

(ii) J_4 and J_5 intervene between two double chains, previously labelled A and B. These two d.c. are shifted such that a dimer of A is in interaction with two dimers of B, as shown in figure 5(a.) They are both held by double SSE paths with nearly similar geometrical features except the M–O–O–M torsion angle ($\sim$70° for J_4 against $\sim$5° for J_5). However, according to figure 5(a) they play a similar role from the point of view of interatomic connectivity, even if the moments connected by J_4 are parallel (+) while those connected by J_5 are antiparallel (−) at the ground state. We decided to constrain them to equal values ($J_4 = J_5$) in spite of geometrical differences in order to simplify the analysis. Strong frustration is expected for particular J_4/J_2 ratios since they are involved in M_1–M_3–M_3 triangles with two moments up ↑ and one moment down ↓. It could be argued that the $J_4 = J_5$ constraint is responsible by itself for an underestimation of their values but attempts to distinguish them in the magnetic phase diagram yields solutions with no clear evidence of regions corresponding to the observed magnetic structure.

(iii) J_3, J_7 and J_8 intervene between two distinct A–C d.c., see figure 5(b). A and C are disposed in a manner such that one dimer of A mainly interact with one facing dimer of C. In fact, after several failing attempts to consider J_8 as an extra parameter, or to constrain it to be equal to other coupling constants, it was finally neglected due to its long associated distance, M–M > 6.2 Å. Despite several geometrical differences, J_3 and J_7 have been constrained to be equal considering their similar role from A to B. In addition, both J_3 and J_7 are involved between parallel magnetic moments.

Then the phase diagram has been calculated for this topology, on the basis of $J_1 = 1$, $J8 = 0$, $-1 \leqslant J_2 \leqslant 1$, $-1 \leqslant J_3 = J_7 \leqslant 1$, $-1 \leqslant J_4 = J_5 \leqslant 1$. In our case, there is no magnetic transition below T_N, so that the first ordered magnetic state characterized by the propagation vector $\mathbf{k} = (1/2, 0, 1/2)$ is also the ground state. The first ordered state is obtained by a calculation done as a function of $\mathbf{k}$ (on the surface or at the interior of the Brillouin zone) and the exchange integrals. This state is given by the eigenvector corresponding to the lowest eigenvalue of the negative Fourier transform of the exchange integral matrix:

$$\xi_{ij}(\mathbf{k}) = -\sum_m J_{ij}(\mathbf{R}_m)\mathrm{e}^{-2\pi \mathrm{i}\mathbf{k}\mathbf{R}_m},$$

where i and j refer to the magnetic atoms in a primitive cell, and $J_{ij}(\mathbf{R}_m)$ is the isotropic exchange interaction between the spins of atom i and j in unit cells separated by the lattice vector $\mathbf{R}_m$ [16–19]. The calculation is performed using ENERMAG. Its principle has been briefly given in the introduction but many more details can be found in [21]. Finally, an auxiliary program uses the output of ENERMAG to plot the 2D plots of phase diagrams using J values as Cartesian axes. Only relative values of J are important for our purposes. Four kinds of ordered domains are found in the investigated zone, including two associated with the target vector $\boldsymbol{k} = (1/2, 0, 1/2)$. Their magnetic characteristics (**k** vector, moments of M_{1-4}) and their corresponding magnetic structures are shown in figure 6.

According to its dominant Mz component, the observed magnetic structure of $BiNiPO_5$ is described by the sequence [$\boldsymbol{k} = (1/2, 0, 1/2)$: (++−−)] and corresponds to the structure labelled as **S2**. All solutions without magnetic ordering, or dominated by incommensurate magnetic structures and frustration effects, are gathered in the domains labelled **S5**. The real nature of the ordering for the exchange integrals defining the **S5** domains may be quite complicated to obtain. A deeper study is needed for each set of J values in order to distinguish between absence of ordering (degeneracy with respect to different k vectors) or incommensurate magnetic ordering.

Figure 7 displays the most representative maps of the different regions of the magnetic phase diagram. Their accurate analysis is quite cumbersome considering the three

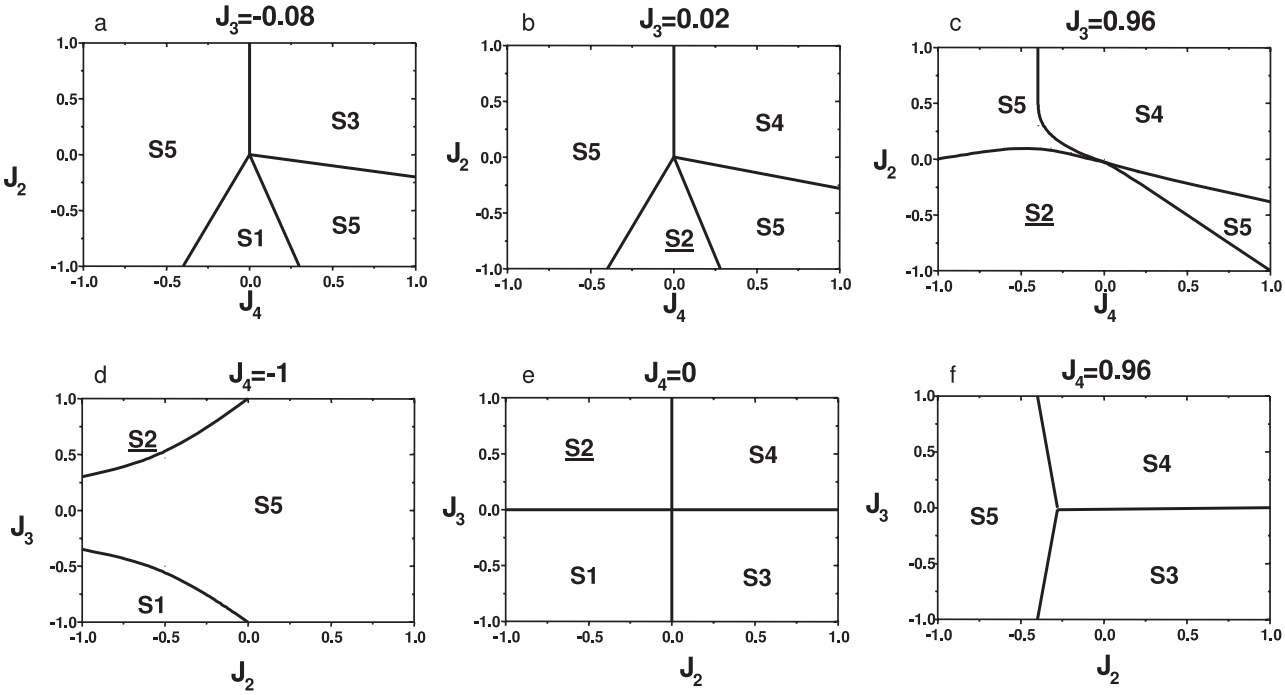

Figure 7. (a)–(f) Maps of the magnetic phase diagram for $BiMPO_5$ (M = Ni, Co). The exchange constant J_1 has been taken as unity ($J_1 = 1$). A systematic variation of J_2, $J_3 = J_7$ and $J_4 = J_5$ in the interval $[-1, 1]$ has been performed. The domains corresponding to the structures **S**1–**S4** are located in the diagram.

variable parameters. Furthermore, the existence of large disordered **S5** domains is an additional clue for the important role that each interaction plays.

Taking into account the number of exchange interactions in competition, their geometrical arrangements and our approximations for the calculation ($J_3 = J_7$, $J_4 = J_5$, $J_8 = J_6 = 0$) of the magnetic phase diagram, it is rather complicated to comment accurately on the maps step by step. We will restrict our investigation to the analysis of the major characteristics of each stable region (**S1**–**S4**):

(i) The refined model, consistent with structure **S2**, involves a negative J_2 (intra double chain) and a positive J_3 (inter double chain) exchange and its expansion in the magnetic diagram mostly depends on the relative J_3/J_4 ratio. Then its size along J_4 is increasing with increasing J_3 values. Figure 7 clearly shows that, for $J_4 = 0$, the observed spin configuration is stable as soon as $J_3 \geqslant 0$. This latter positive J_3 combined with negative J_2 should have a predominant role compared to J_4 that may be estimated as much weaker.

(ii) The analysis of the structure **S1** is all the more informative since it does not modify intra d.c. ordering nor inter A–B d.c. ordering. However, the inter A–C ordering is shifted along c compared to the structure **S2**. The comparison of figures 7(a) and (b) and the examination of figure 7(c) clearly shows the modification of structure **S2** to structure **S1** on reversal of the sign of J_3, negative for the latter structure **S1**.

(iii) Both structures, **S3** and **S4**, involve a magnetic ordering in the crystallographic unit cell, corresponding to $\mathbf{k} = (0, 0, 0)$. As expected from figure 7, the structure **S3** implies positive J_4, negative J_3 and weakly negative to strongly positive J_2 inter-dimeric exchange. As a matter of fact, the ferromagnetic structure **S4** arises on J_4 reversal into a positive value (and even weak negative J_4 values for strongly positive J_3).

(iv) Disordered domains **S5** are mostly driven by particular J_3/J_4 ratios. Indeed two J_4 and one J_2 are involved in a M1–M3–M3 triangle. Then it appears that, for weak values for J_3, the **S5** domain predominates in the J_2 versus J_4 maps as soon as at least one of them is negative.

The case of Co^{2+} deserves a special comment since, as already discussed, it is well known that this ion in a high spin state presents a relatively strong spin–orbit coupling. This is the reason why both $\mu_{\text{eff}} = 5.40\mu_B$ and $m_{1.5\,K} = 3.52\ \mu_B$ are greater than expected. The resulting anisotropy gives the explanation why the collinearity of the magnetic structure is largely lost for this compound. However, if we consider the larger Mx component and the weaker Mz of the moment, the sequence of signs $C = (++--)$ remains valid as well as the analysis of the diagram developed in the M = Ni case. Comparable behaviour has already been reported for cobalt, in the $M^{2+}Fe^{3+}PO_5$ (M = Fe, Co, Ni, Cu) systems [21]. The magnetic anisotropy of cobalt is such that the $Co^{2+}Fe^{3+}PO_5$ magnetic structure is defined with basis functions $[0, Cy, Gz]$ for Co^{2+} and $[0, 0, G'z]$ for Fe^{3+}, while the three $M^{2+}Fe^{3+}PO_5$ other compounds show collinear magnetic structures with basis functions $[0, Gy, 0]$ for M^{2+} and $[0, G'y, 0]$ for Fe^{3+}. In that case too, the main component of the magnetic moments is associated with the same $G = [+-+-; +-+-]$ sequence

of signs for all compounds (M = Fe, Co, Ni, Cu) in the series. A complete analysis should include the single-ion anisotropy terms as well as anisotropic exchange interactions of lower orders of magnitude.

7. Conclusion

The magnetic structures of $BiMPO_5$ (M = Ni, Co) compounds have been refined using the Bertaut group theory analysis by means of neutron diffraction below T_N. The same magnetic structure, $\mathbf{k} = (-1/2, 0, 1/2)$, that can be described by the irreducible representation Γ_2 has been found for M = Ni and Co:

$$\Gamma_2 : C^X = S_1^X + S_2^X - S_3^X - S_4^X;$$
$$A^Y = S_1^Y - S_2^Y - S_3^Y + S_4^Y;$$
$$C^Z = S_1^Z + S_2^Z - S_3^Z - S_4^Z$$

with S_{1-4} related to the four M_{1-4} positions by primitive unit cell. For M = Ni ($m_{1.5\,K} = 2.13(3)\ \mu_B$), the magnetic moments are nearly collinear to z ($m_z \gg m_x, m_y$) while for M = Co ($m_{1.5\,K} = 3.52(3)\ \mu_B$) the collinearity is largely lost ($m_x > m_y > m_z$) due to the strong magnetic anisotropy reminiscent of the large orbital contribution for high spin Co^{2+}, although, taking into consideration the predominant magnetic component as arising from the isotropic exchange interactions, both compounds respect the same (++−−) sequence. For the calculation of the magnetic phase diagram available in both cases, the large number of interplaying interactions has been reduced to one J_1 M–O–M and three J_{2-4} M–O–O–M super–super-exchange interactions, on the basis of geometrical considerations. The refined magnetic structure available at the ground state is stable for particular $J_2/J_3/J_4$ ratios while large disordered domains have also been shown due to the competition between positive and negative super–super-exchange interactions.

References

[1] Abraham F and Ketatni M 1995 *Eur. J. Solid State Inorg. Chem.* **32** 429
[2] Ketatni M, Abraham F and Mentré O 1999 *Solid State Sci.* **1** 449
[3] Xun X, Uma S and Sleight A W 2002 *J. Alloys Compounds* **338** 51
[4] Xun X, Uma S, Yokochi A and Sleight A W 2002 *J. Solid State Chem.* **167** 245
[5] Ketatni M, Mernari B, Abraham F and Mentré O 2000 *J. Solid State Chem.* **153** 48
[6] Ketatni M, Huvé M, Abraham F and Mentré O 2003 *J. Solid State Chem.* **172** 327
[7] Colmont M, Huvé M, Abraham F and Mentré O 2004 *J. Solid State Chem.* **171** 4149
[8] Abraham F, Cousin O, Mentré O and Ketatni E M 2002 *J. Solid State Chem.* **167** 168
[9] Colmont M, Huvé M and Mentré O 2006 *Inorg. Chem.* **45** 6612
[10] Huvé M, Colmont M and Mentré O 2006 *Inorg. Chem.* **45** 6604
[11] Colmont M, Huvé M, Ketatni M and Mentré O 2008 *Solid State Sci.* **10** 533
[12] Huvé M, Colmont M and Mentré O 2004 *Chem. Mater.* **16** 2628
[13] Mentré O, Ketatni M, Colmont M, Huvé M, Abraham F and Petricek V 2006 *J. Am. Chem. Soc.* **128** 10857
[14] Ehora G, Daviero-Minaud S, Colmont M, André G and Mentré O 2007 *Chem. Mater.* **19** 2180
[15] Elbouaanani L K, Malaman B, Gérardin R and Ijjaali M 2002 *J. Solid State Chem.* **163** 412
[16] Yoshimori A 1959 *J. Phys. Soc. Japan* **14** 807
[17] Villain J 1959 *J. Phys. Chem. Solids* **11** 303
[18] Lyons D H and Kaplan T A 1960 *Phys. Rev.* **120** 1580
[19] Freiser M J 1961 *Phys. Rev.* **123** 2003
[20] Warner J K, Cheetham A K, Cox D E and Von Dreele R 1992 *J. Am. Chem. Soc* **114** 6074
[21] El Khayati N, Cherkaoui R, Moursli El, Rodríguez-Carvajal J, André G, Blanchard N, Bourée F, Collin G and Roisnel T 2001 *Eur. Phys. J.* B **22** 429
[22] El Khayati N, Rodríguez-Carvajal J, Bourée F, Roisnel T, Cherkaoui R, Boutfessi A and Boukhari A 2002 *Solid State Sci.* **4** 1273
[23] Rousse G, Rodríguez-Carvajal J, Wurm C and Masquelier C 2001 *Chem. Mater.* **13** 4527
[24] Rousse G, Rodríguez-Carvajal J, Wurm C and Masquelier C 2002 *Solid State Sci.* **4** 973
[25] Rousse G, Rodríguez-Carvajal J, Patoux S and Masquelier C 2003 *Chem. Mater.* **15** 4082
[26] Dai D, Whangbo M H, -Koo H J, Rocquefelte X, Jobic S and Villesuzanne A 2005 *Inorg. Chem.* **44** 2407
[27] Rodríguez-Carvajal J 1993 *Physica* B **192** 55 The programs of the *FullProf Suite* and their corresponding documentation can be obtained from the Web at http://www.ill.eu/dif/software
[28] Nadir S, Swinnea J S and Steinfink H 1999 *J. Solid State Chem.* **148** 295
[29] Bertaut E F 1971 *J. Physique* **32** C1
[30] Rodríguez-Carvajal J 2004 *BasIreps: a Program for Calculating Irreducible Representations of Little Groups and Basis Functions of Polar and Axial Vector Properties* (Grenoble: ILL)
[31] Anderson P W 1952 *Phys. Rev.* **86** 694